Construction and Building Materials 310 (2021) 125168

Contents lists available at ScienceDirect

Construction and Building Materials

journal homepage: www.elsevier.com/locate/conbuildmat

Self-healing efficiency of Ultra High-Performance Fiber-Reinforced Concrete through permeability to chlorides

Hesam Doostkami [a,*], Marta Roig-Flores [b], Pedro Serna [a]

[a] ICITECH - Institute of Concrete Science and Technology, Universitat Politècnica de València, 4N Building, Camino de Vera s/n, València, Spain
[b] Department of Mechanic Engineering and Construction, Universitat Jaume I, Av. Sos Baynat s/n, Castelló de la Plana, Spain

ARTICLE INFO

Keywords:
Ultra-High-Performance Fiber Reinforced Concrete
Self-healing
Autogenous healing
Crystalline Admixture
Water Penetration
Chlorides

ABSTRACT

This study presents a novel methodology to evaluate the self-healing capability of Ultra High-Performance Fiber-Reinforced Concrete (UHPFRC) designed to compare conventional concrete types. The procedure used combines loading reinforced concrete elements until a fixed strain level to have a comparable total crack opening. Afterwards, water penetration to chlorides is used as an indicator of permeability. This work compares autogenous healing efficiency of a conventional concrete, a high-performance concrete, and two types of UHPFRCs with and without 0.8% of a crystalline admixture (CA) by the binder weight. The results show that all UHPFRC specimens exhibited excellent autogenous healing, higher than conventional concretes for an equivalent total crack. The self-healing results depended greatly on the crack size and the fiber content. Additionally, UHPFRCs with CA obtained the lowest water permeability after promoting self-healing for one month in water immersion and presented almost complete healing against chloride penetration.

1. Introduction

1.1. Background

In reinforced concrete structures, cracks can create a path for aggressive agents towards the structure's interior, deteriorating its lifespan and durability [1]. In general, cracks until 50 μm are considered to have a non-significant effect on the permeability, while cracks until 200 μm can accelerate the water permeability [2]. However, structural codes such as Model Code 2010, Eurocode 2, 1992 or BS 8110-1, 1997, allow cracks under 300 μm depending on the environmental condition (unless specific requirements such as water tightness have to be met). Other factors that can also influence the element's permeability [3], such as the shape, tortuosity, and crack direction, are usually not considered.

Some reinforced concrete structures that suffer early or unexpected cracking, could need repair actions in order to prevent a fast penetration of aggressive agents and to avoid further degradation. Repairing cracks is not always an easy solution, and it could involve stopping the service that the structure provided, traffic cuts, among other costs. In some cases, self-healing concrete could be a cost-effective option when compared to repairing cracks, and a possible way to extend the structure's service life and to decrease maintenance costs [4].

Concrete can seal its own cracks to some extent by autogenous healing, recovering some properties as a result [1]. This process is produced mainly by the hydration of un-hydrated cement particles and precipitation of calcium carbonate crystals on the surface as a reaction between portlandite and carbonate ions or carbon dioxide [5]. The properties that can be recovered by self-healing are crack closure, durability properties (typically water permeability), and mechanical properties [6].

In the last years, several self-healing agents have been proposed to promote self-healing, such as Crystalline Admixtures (CA) [1], to improve the low capability of autogenous healing in conventional concretes [7]. CA are classified as a particular type of permeability-reducing admixtures (PRAs) by the ACI Committee 212 [8], which are also thought to promote self-healing of small cracks below 0.4 mm. These admixtures are hydrophilic and react with water, cement, and $Ca(OH)_2$ to form calcium silicate hydrates and other precipitates [9]. Using CA in conventional concrete types has shown slight enhancements in their self-healing capacity [10–15].

* Corresponding author.
E-mail address: hedoo@doctor.upv.es (H. Doostkami).

https://doi.org/10.1016/j.conbuildmat.2021.125168
Received 14 July 2021; Received in revised form 7 September 2021; Accepted 4 October 2021
Available online 19 October 2021

1.2. Self-healing in UHPFRC

Ultra-High-Performance Fiber Reinforced Concrete (UHPFRC) is an advanced cementitious material known for its self-compacting behavior, excellent mechanical properties [16], and very low permeability due to its dense matrix and low water/cement ratio [17]. The strength of UHPFRCs is around 135 to 200 MPa in compression and 7 to 15 MPa in tension. Furthermore, UHPFRC has a strong multi-cracking response thanks to the deflection-hardening and, often, strain-hardening behavior due to the high contents of fibers [18]. UHPFRC exhibits a post-crack pattern with multiple microcracks, and only close to failure, some of them are developed into macrocracks (>50 μm) [19].

In uncracked conditions, UHPFRC has excellent durability and transport properties. The porosity accessible to water in UHPFRCs at 28 days can be 7-fold lower than in a concrete of class C30 and 4-fold than in a concrete class C90 [20]. Similarly, the oxygen permeability can be three orders of magnitude lower than in a C30 and one order of magnitude lower than in C90 [20]. Additionally, conventional concrete's chloride diffusion can be 3 times and 78 times higher than HPC and UHPFRC, respectively [21].

Some authors investigated water permeability of UHPFRC in cracked conditions. One study [17] showed experimental results of pre-cracked elements up to several levels of residual strain. The results showed that until a residual strain of 1.3‰, which resulted in a total crack of 130 μm in 100 mm length specimen, the water permeability coefficient of UHPFRC was practically not affected. The results also indicated that, above that threshold, higher strain values led to increasing water permeability coefficients. Another study [22] that tested UHPFRC water permeability in cracked conditions obtained no water movement through 25 μm cracks even using high pressures and only a few grams of water in 50 μm size cracks. For conventional concrete types, 50 μm is usually considered as the threshold crack opening [23] and cracks thinner than this level are deemed not to affect the permeability to water.

Due to the high amount of anhydrous cement particles and its cracking pattern with narrow microcracks, UHPFRC may experience enhanced autogenous healing in the presence of water [4,24]. In fact, introducing fibers in conventional concrete (55 MPa) already produces concrete with 60 to 70 % lower permeability in cracked state and higher self-healing capability than conventional concrete (35 MPa) [25] due to the smaller size of the cracks.

Crystalline admixtures may respond differently in UHPFRC due to their higher binder content and low w/b ratio. One study reported that CA enhanced self-healing in UHPFRC and standard strength concrete using flexural strength recovery and suggested a "chemical prestressing effect" as synergy between the fibers and CA [9]. Another study [26] observed similar mechanical behavior in HPFRC with and without CA. However, HPFRC with CA presented more stable self-healing results and better mechanical recovery, which was also suggested to be produced by a collaboration between fibers and CA to the formation of self-healing product [26].

1.3. Penetration of chlorides through healed cracks

Crack healing has been reported to reduce water permeability and to recover water tightness; however, that does not necessarily imply that healed cracks are able to protect from the penetration or diffusion of chlorides, which could initiate the corrosion of the steel reinforcement.

Regarding the diffusion of chlorides through healed cracks, one study [27] reported that in a conventional concrete, cracks smaller than 60 μm are able to heal and protect against chloride diffusion, while broader cracks experienced only partial self-healing. Another study [28] showed that for small cracks (lower than 60 μm), the age of the crack influences the capability of self-healing to impede chloride diffusion, with younger cracks (produced at the age of 28 days) obtaining better results than older cracks (2 years) [28]. However, for larger cracks, the cracking age appeared to have no significant effect [28]. That same study indicated 30 μm as a critical mechanical opening [28], indicating that for smaller crack openings, no chloride diffusion occurs along the crack path.

Other studies evaluated chloride penetration through pigmentation with silver nitrate ($AgNO_3$), which is a low-cost, straightforward and reliable technique for measuring chloride penetration in every type of concrete [29–31]. One study [32] pointed out 13 μm as the necessary crack width to stop the chloride penetration of samples immersed in artificial seawater. Similarly, another study [2] obtained that cracks of 105 μm were able to heal autogenously, and cracks>105 μm were only partially healed, not providing resistance against the penetration of chlorides, while 10 μm was detected as the critical crack width to limit the chloride penetration.

1.4. Current limitations and approach of this work

There are no standards yet for the evaluation of self-healing in concrete. Water permeability has been extensively tested in conventional concrete and fiber reinforced concrete to evaluate the self-healing performance. The strict comparison between water permeability of conventional concrete and UHPFRC is still a challenge since the permeability coefficient of uncracked UHPFRC is lower than the limit of detection in some methodologies [17,22].Moreover, their differences in the crack pattern (crack length, crack distribution, tortuosity) are an additional challenge to ensure fair comparison at comparable damage levels.

This work aims to compare the self-healing efficiency of UHPFRC elements with very low water permeability in cracked conditions with conventional concrete types without fibers by using the same test and parameters. To this purpose, steel reinforcement will be included to control the deformation and cracking processes, which will allow testing different concrete types, including those without fibers, and thus adding as a variable the type of concrete. In this research, four concrete mixes are studied: a conventional concrete, a high-performance concrete, and two types of UHPFRC. These mixes will be cast into reinforced specimens and pre-cracked by 4-point bending test, until two levels of residual strain, which will represent two levels of damage, one inside the serviceability limit state and another close to the ultimate limit state. The crack patterns produced in the four concrete types will be different, with single-macrocracks in the conventional and high-performance types and narrow multi-microcracks in the UHPFRCs. The use of 4 point-bending test will allow the extraction of samples from the central span of the beams, which theoretically will have experienced constant bending stresses. These samples will have associated a strain value that will represent the structural material response. By using strain instead of the value of total crack width (sum of the individual cracks), the effect of very thin cracks that are not detectable visually is also included.

Self-healing will be then tested in these samples using a chloride penetration test with silver nitrate to evaluate their water penetrability before and after healing.

The method proposed in this work allows the evaluation of the self-healing efficiency of cracked UHPFRCs elements, as compared with conventional concretes, and the influence on self-healing of the strain level, expected crack pattern, and matrix porosity can be considered. Additionally, this work also evaluates the efficiency of a crystalline admixture in the two UHPFRCs to improve self-healing in terms of water penetration using the same methodology.

2. Materials and methodology

2.1. Materials

Four concrete mixes were studied in this work, named C1, C2, C3, and C4. C1 is a conventional concrete (C30/37), and C2 is a High-Performance Concrete (C70/85). C3 and C4 are two Ultra-High-

Performance Fiber Reinforcement Concrete (UHPFRC) mixes with different sand size distribution and different steel fiber content. Additionally, two enhanced versions of C3 or C4 UHPFRCs with crystalline admixture were prepared to study its influence on self-healing in those mixes, which were named C31 and C41, respectively.

The binder components used are cement type CEM I 42.5 R-SR5 from Lafarge and un-densified micro-silica from Elkem. Superplasticizer ViscoCrete-20 HE from Sika was used in C2, C3, and C4 mixes, while no superplasticizer was used in C1.

In C1 and C2 mixes, typical crushed 7/12 and 4/7 aggregates and natural sand were used. In C3 and C4 mixes, the aggregates used were (0/0.5 mm) and (0/1.6 mm) silica sand and silica flour Quarzfin U-S 500 from Sibelco.

The C3 and C4 mixes incorporated short straight-shaped steel fibers 13/0.2 (length 13 mm, $\Phi = 0.2$ mm, $l_f/d_f = 13/0.2 = 65$, tensile strength > 2000 MPa), to guarantee ductility and multiple micro-cracking. Penetron ADMIX was used as a crystalline admixture. Penetron Admix is made of Portland cement and various active chemical formulations, which produce a catalytic reaction when in contact with moisture in fresh concrete and by-products of cement hydration. This chemical reaction generates a non-soluble crystalline formation throughout the pores and capillary tracts of the concrete that permanently seals micro-cracks against the penetration of water or liquids. The dosage used complies with the supplier recommendation of 0.8–1.0% by the weight of the binder. Table 1 shows the composition of the six concrete mixes and the code used for this work.

All specimens cast were demolded 24 h after mixing and were kept in a humidity chamber at 20 °C and 95% relative humidity until their testing time.

These mixes were characterized through compressive strength (EN 12390–3) at the age of 28 days in cylinders of 150 mm of diameter and 300 mm height in C1 and C2 mixes and 100 mm cubes for C3, C31, C4, and C41 mixes. The results obtained are displayed in Table 1.

To fully characterize UHPFRC mixes (C3, C31, C4, and C41), two prisms of size 100x100x500 mm^3 were prepared to test at four-point bending on unnotched specimens. After performing the four-point bending test, tensile properties were evaluated following the Simplified Inverse Analysis method from [33–35]. The results obtained after completing the Inverse Analysis are displayed in Table 1.

The results show that C4 had a slightly lower mechanical performance than C3, as expected due to its lower fiber content. The crystalline admixture introduction in C3 and C4 mixes led to decreased compressive strength and tensile strength properties.

Table 1
Mix designs of Conventional, High Performance, and UHPFRCs.

kg / m³	C1	C2	C3	C31	C4	C41
Cement I 42.5 R-SR	350	450	800	800	800	800
Silica Fume	0	50	175	175	175	175
Water	207	160	160	160	160	165
w/c	*0.591*	*0.356*	*0.200*	*0.200*	*0.200*	*0.206*
w/b	*0.591*	*0.320*	*0.164*	*0.164*	*0.164*	*0.169*
Aggregate 7/12	600	200	–	–	–	–
Aggregate 4/7	300	600	–	–	–	–
Natural sand	950	950	–	–	–	–
Limestone filler	60	–	–	–	–	–
Silica sand – 1.6 mm	–	–	565	565	–	–
Silica sand – 0.5 mm	–	–	302	302	1092	1092
Silica flour	–	–	225	225	–	–
Short steel fibers (13/0.2)	–	–	160	160	130	130
Superplasticizer Sika 20 HE	–	3.5	30	30	30	30
PENETRON ADMIX	–	–	–	7.8	–	7.8
$f_{cm,28d}$ ***(MPa)***	38.97	82.75	149.50	119.39	121.11	113.31
f_t ***(MPa)***			9.73	7.61	8.46	7.30
f_{tu} ***(MPa)***			8.54	6.64	7.88	6.08
ϵ_{tu} ***(‰)***			4.23	1.81	3.17	2.37

2.2. Self-Healing methodology

2.2.1. Beam's geometry and reinforcement

Reinforced beams sized 100 × 150 × 750 mm^3 (Fig. 1) were prepared for the self-healing evaluation. Two beams per mix were evaluated. These beams were reinforced with 2ø8 lower rebars and 6ø6 stirrups to control the cracking process and minimize the possibility of shear failure.

2.2.2. Pre-cracking process

The four-point bending test setup consists of a span of 600 mm between support and 150 mm distance between the loading points. Two rows of points used to measure by demountable mechanical strain gauge (DEMEC points) placed, one at the lower rebars level and the other at the medium height of the beam, were glued at the central part of the beam (Fig. 1) for controlling the strain variation at these two levels, before, after, and during the loading–unloading cycles. Each DEMEC point was placed at a distance of 50 mm, and the measurements were performed using alternate points, that is, always using a length of 100 mm. Furthermore, to record the load–deflection, a Linear variable differential transformer (LVDT) was placed under the beam in the central section. Two couples of beams were prepared for each mix (24 reinforced beams in total) to be pre-cracked in two residual strain levels: LS (Low Strain) and HS (High Strain).

Fig. 2 shows an example of load–deflection curves obtained under the 4-point bending test setup described for the reinforced concrete (RC) beams of UHPFRC and conventional concrete. UHPFRC beams reached significantly higher loads and stiffer response if compared with the RC beam with conventional concrete. After an initial formation of cracks in UHPFRC, the material keeps producing and propagating new micro-cracks. On the contrary, in Conventional and High-Performance concrete, few cracks grow wider following a discrete crack pattern.

The creation of controlled crack opening is a necessary step to analyze the self-healing capability of the concrete specimen before and after self-healing and to compare it between beams of different materials. Using reinforcement allowed controlling the cracking process and achieve the desired cracking level in the central area. Using large beams permitted to obtain a multi-crack pattern in the central area of the specimen in a larger space, facilitating the formation of the different crack patterns and the localization of every single crack.

With this pre-cracking setup, the RC beams could be loaded until reaching the same residual strain range in order to have a limited range of total crack opening. With the pre-cracking method described, two levels of damage (that is, average/equivalent strain) were produced in the beams:

a) Low strain (LS): is considered achieved when the beam reaches an average strain $\geq$ 0.5‰ (0.05 mm /100 mm) at the mid-height DEMEC row in loaded conditions. This limit is still in the elastic branch in steel. This strain level represents a condition close to the serviceability limit, where small cracks are appearing and will be very thin after removing the load.
b) High strain (HS): is considered achieved when the beam reaches a residual strain between 1‰ and 2‰ (0.10–0.20 mm /100 mm) after unloading at the lower DEMEC row. This point corresponds with a residual strain equal to the expected yielding strain of steel rebars and the maximum concrete strength. This strain level represents a condition close to the ultimate limit state.

A series of loading–unloading steps are performed until obtaining the desired residual strain. Fig. 3 presents two examples of the load–strain levels reached during the loading and unloading steps in the two mentioned groups. The black points show the values obtained for the bottom row of DEMEC points, while the gray points show the values obtained for the middle row of DEMEC points. For LS samples, the strain needed at the middle row of DEMEC points (black curves) is usually

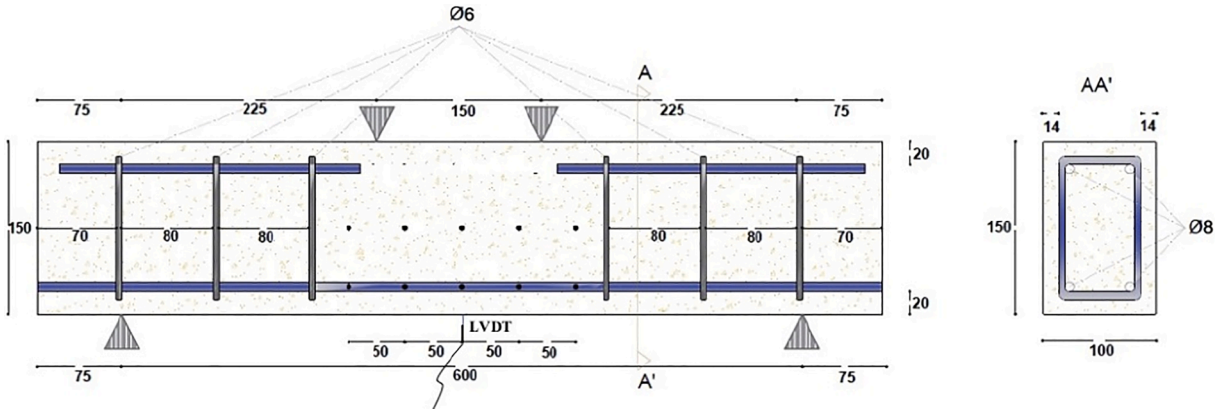

Fig. 1. Reinforced Beam model and DEMEC point locations (mm).

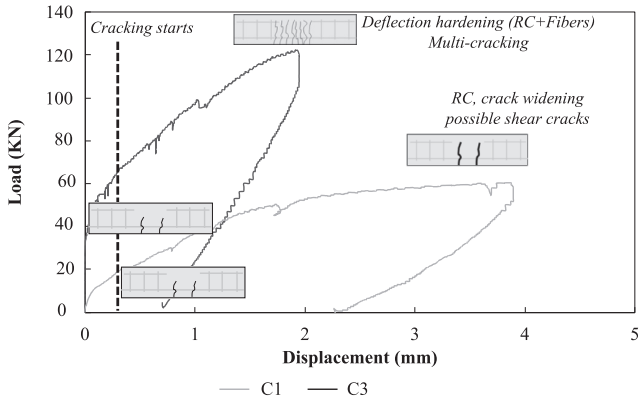

Fig. 2. Stress-defection responses of beams of a conventional concrete C1(grey) and a UHPFRC C3 (black).

reached during the first load step. The graph also shows that after unloading, most of the strain is significantly reduced in this group. In the HS samples, 2 or even 3 cycles of loading-reloading were needed to reach the desired residual strain level in the bottom row after unloading.

2.2.3. Preparation of specimens for the self-healing evaluation

After the pre-cracking procedure, all the beams were cut into four smaller prisms sized 150 × 150 × 50 mm^3, as presented in Fig. 4. These prisms were named A, B, C, and D. The four prisms were assumed to have the same deformation since the cracks were gathered in the middle area of the beam due to the pre-cracking setup. The prisms were sawed following the lines displayed in Fig. 4.

The method performed to evaluate water penetration using chlorides penetrations cannot be repeated in the same specimen two times at different ages since the test is destructive. Because of this, to analyze self-healing efficiency, half of the samples were selected to evaluate the properties without a healing process, and half of the samples were evaluated after healing.

2.2.4. Crack analysis

In order to measure the crack size of the samples, a PCE-MM200 USB optical microscope was used, together with a concrete crack-meter as a size reference. In the HS samples, cracks were large enough to be measured by the naked eye, but in the LS samples, cracks were only visible by using the microscope.

The two rows of DEMEC points where the strain was measured were observed with the microscope using a magnification of 200X. All the cracks were counted, located, and photographed. A crack-meter was used as the reference picture, and the photos of the sections were analyzed using Adobe Photoshop. In this way, crack number, crack size,

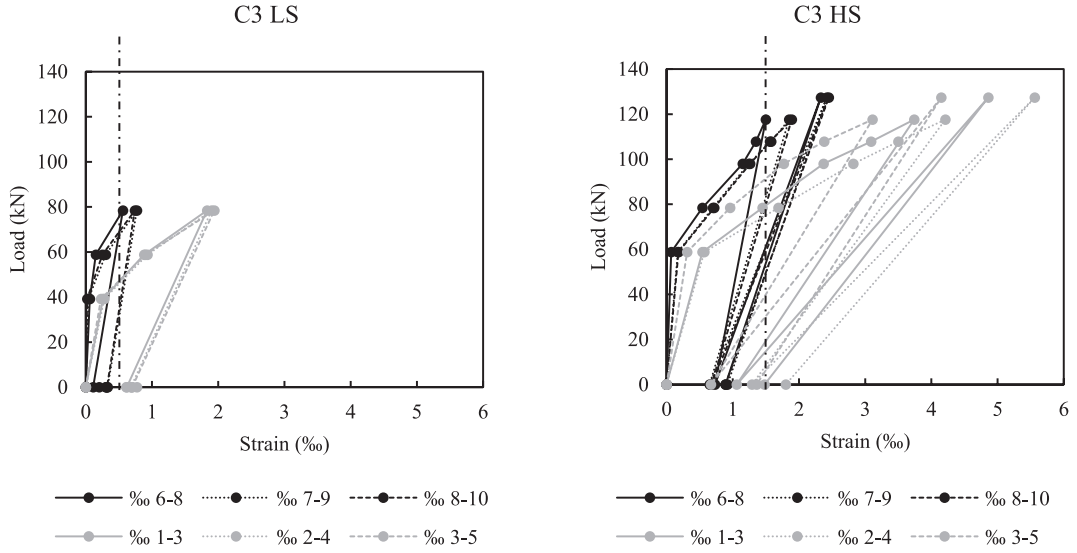

Fig. 3. Load-strain curves of each DEMEC point interval (E.g., 6–8 ‰ means strain between points 6 and 8) in a C3 sample during pre-cracking in the Low Strain (LS) (left) and High Strain (HS) (right) levels.

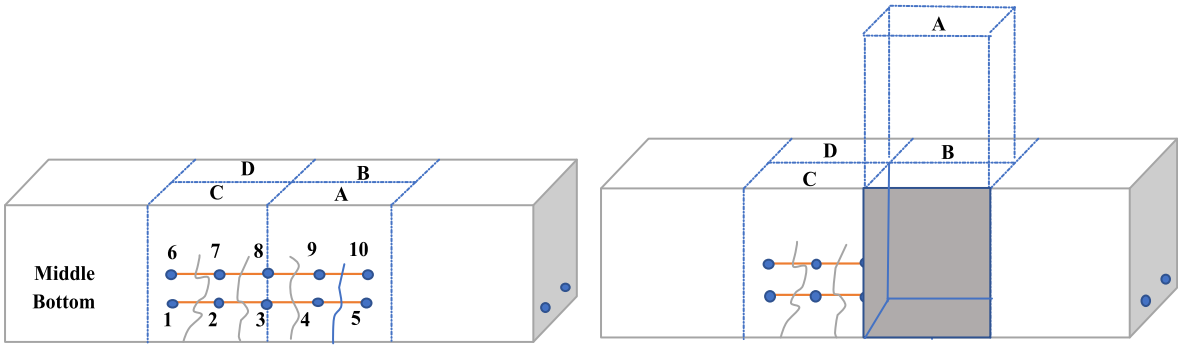

Fig. 4. Diagram of the beam presenting the sawing lines to obtain the self-healing samples.

and crack locations for both measuring lines can be compared with the strain obtained at these lines through the DEMEC during the pre-cracking stage.

During these measurements, it was detected that some cracks were healed partially or entirely before they were immersed in water. This healing happened especially in those samples with a crack width lower than 0.05 mm.

2.2.5. *Water penetration through a chloride penetration test*

Previous research showed the problems of measuring water flow in UHPFRC due to its low permeability even in cracked conditions [22]. This problem was coherent with other results in the literature [17 16], which also indicated that 50 μm as a threshold width affects the permeability in standard concrete and UHPFRC strain levels of 1.3‰ (total crack of 130 μm) showed no significant effects on permeability.

Due to these difficulties, a modified water penetration test was conducted by measuring the penetration of water with sodium chloride through the cracks by using its reaction with silver nitrate as a pigmentation method to detect the areas where water penetrated.

The test setup used to evaluate the penetration of water consists of gluing PVC tubes with an outer diameter of 75 and height of 60 cm using a resin (Sikaflex 11 FC) over the small sawed specimens. The tubes were glued to cover the two DEMEC lines, as presented in Fig. 5. These tubes were filled with 50 cm of water with a concentration of 35 gr/liters of regular salt as sodium chloride). It needs to be mentioned that the bottom surface of the specimen was not sealed since the water permeability of UHPFRC samples in these conditions is almost zero [22]. The water column was left for three days. Afterward, the water in the tubes was removed, and the tubes were also un-glued. After one day of drying at laboratory conditions, the samples were sawed by a circular concrete saw again from the DEMEC line at the middle section of the sample (perpendicularly to the cracks). The sample was sawed with a wet cut and making sure that the cut direction was going from the side that was not in contact with the water with salt towards the side that was in contact in order to reduce the contamination of the section during the cut.

After the cut, the samples were left to dry for a day. Then, a silver nitrate ($AgNO_3$) solution with a concentration of 0.1 mol/l was sprayed on both surfaces. When spraying an element with $AgNO_3$, two pigmentation areas emerge: the dark areas indicate the regions without chlorides (the reaction of silver ions with hydroxyls) while the white areas indicate the regions containing chlorides (reaction of silver ions with chloride ions), and thus, the regions with corrosion risks for the steel reinforcement [29,36,37]. In order to have more clear white-dark color boundaries, studies like [29,36,38] have recommended using the concentration of 0.1 N silver nitrate (equals 0.1 mol/l).

After spraying samples with silver nitrate, they were put into the oven at 80 °C for 24 h to improve the pattern display. The photos of the specimens after the reaction of $AgNO_3$ were taken by a Digital Camera. Each picture was then converted to binarized black and white using photography software (Adobe Photoshop) to highlight the penetration area.

These images showing the penetration in each half of the sawed sample can show the depth of penetration and its location to study the degree of chloride penetration in each specimen. Since the crack number, crack size, and the residual strain of this location had been

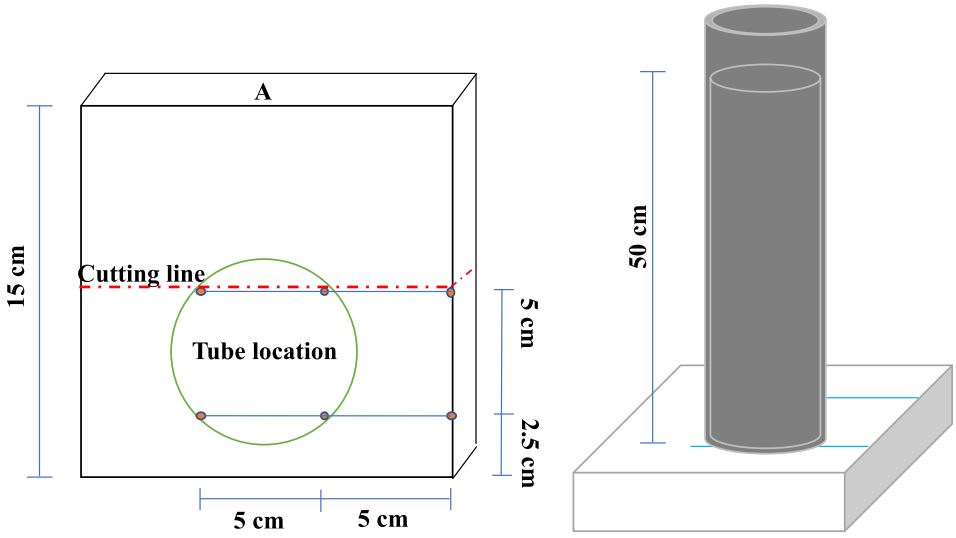

Fig. 5. Tube location and cutting line for the water penetration test based on chloride penetration.

evaluated, the penetration of chloride can gather comprehensive results in the mentioned location.

Fig. 6 shows two example pictures of the cut section after the silver nitrate reaction, one from a conventional concrete (top picture) and another from a UHPFRC concrete, and their respective binarized image.

Different penetration types were detected in the samples: penetration through the matrix (P_0) and penetration through the crack branches. Most crack branches connected the whole width of the sample, which indicated that water could move inside the width of the sample.

In conventional concrete samples, P_0 was very clear and easy to measure, while in HPC and UHPFRC samples, P_0 was very small due to their lower matrix porosity, which complicated its exact evaluation due to the precision limits of the method.

In each crack branch, the penetration width of each branch and penetration depth can be measured. The penetration branches had nearly the same width along the width of the sample, then to measure the parameter named "penetration width," the average of three equidistant points was evaluated (Fig. 6.). For the conventional concrete samples, the crack branches were conical, making it impossible to clearly differentiate them from P_0 penetration. It should be mentioned that C1 and C2 samples with HS had visible cracks and are not adequate to perform this chloride penetration test due to the leakage of water. Therefore, the conventional and high-performance samples were not evaluated for HS strain level by this test, and only LS samples were tested by this method to be compared with UHPFRC samples.

In UHPFRC (C3, C31, C4, and C41), the crack branches were much more widespread and larger than the crack width measured by the microscope, which suggests the presence of branches of internal microcracks or the accuracy limit of the method.

The photos obtained showed differences between samples healed during 28 days in deionized water and the unhealed reference samples. Consequently, all samples' photos were analyzed to measure their unhealed and healed parameters obtained from the chloride penetration pattern. Self-healing can be evaluated through the "Healing ratio" described in Eq. (1), by using the value of the specific parameter in healed and unhealed conditions. 28-day old unhealed samples were measured just after sawing.

$$Healing\ \ ratio = 1 - \frac{\text{Healed parameter}}{\text{Unhealed parameter}} \tag{1}$$

2.2.6. Self-healing condition

As the environmental condition to promote self-healing reactions a tank full of deionized water was prepared. This deionized water was obtained from cationic and anionic resin (60% anionic of a strong base

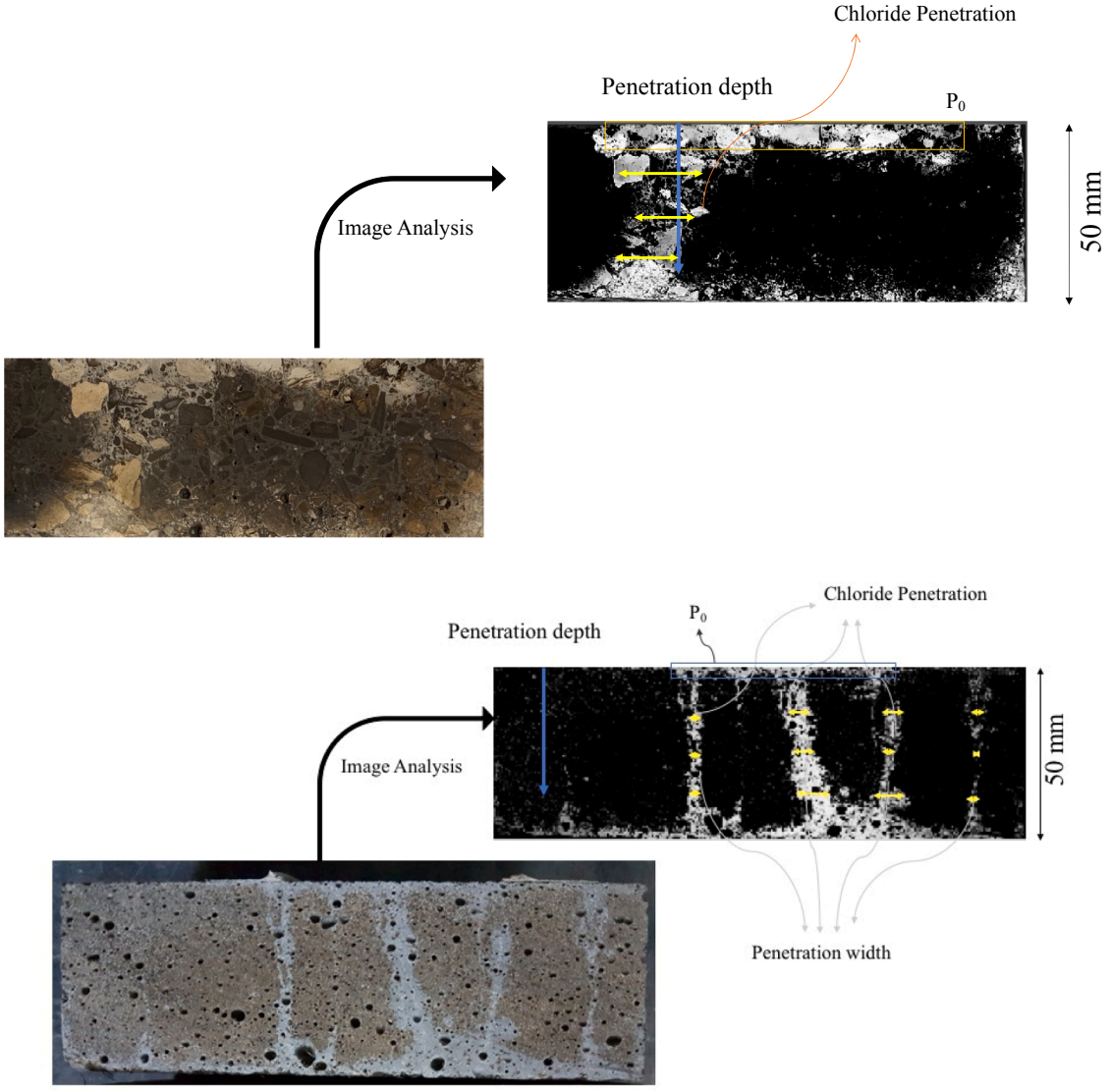

Fig. 6. Process of an image analysis in a conventional concrete sample (top photo) and in a UHPFRC sample (bottom photo).

and 40% cationic of a strong acid). Deionized water was selected in order to avoid potential impacts of contamination by the potential minor presence of chlorides in tap water. Their presence was expected of little influence, but it could affect the results since the penetration was also expected to be very small in UHPFRC samples.

At the same age, when samples are tested to obtain the values of an unhealed couple, the twin of each sample were immersed in the tank with deionized water at room temperature for 28 days to heal. After 28 days of healing submerged in water, healed samples were brought out from the tank, and after a day of drying in laboratory conditions, cracks dimensions and chloride penetration were evaluated.

3. Results and discussion

3.1. Pre-cracking results

The results obtained from the pre-cracking test are displayed in the load–displacement graphs in Fig. 7.

C3 samples reached the highest load (~12 tons) when reaching the residual target strain due to its higher flexural strength, higher than C4

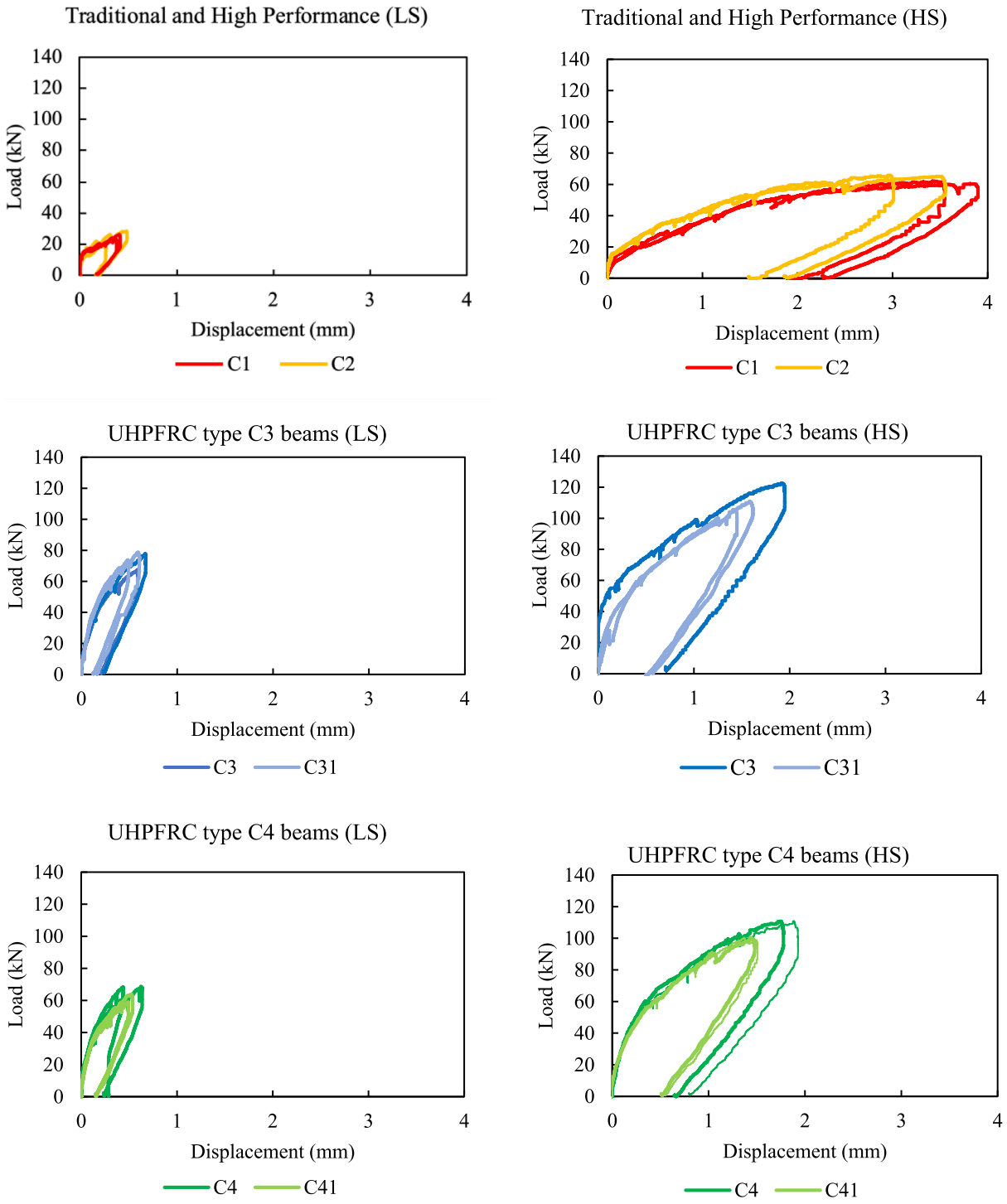

Fig. 7. Load vs. vertical displacement curves of C1, C2, C3, and C4 obtained from the pre-cracking stage of the beam for LS (left column) and HS strain (right column) levels.

samples due to the higher fiber content. The presence of crystalline admixture in C3 and C4 reduced the load at the target residual strain.

For conventional (C1) and high-performance (C2) concretes, the flexural strengths were low, reaching the target strains at loads lower than 60 kN. Due to the difficulties in controlling the deformation in these samples, some beams reached higher strains (3‰ and 4‰).

3.2. Strain and crack width relation

Table 2 displays the values obtained from the pre-cracking test for the beams tested, including for the two levels (bottom and middle), residual strain, average crack width, number of cracks (in the detectable range), and total crack width, calculated as the sum of the individual cracks.

The values obtained from the bottom DEMEC line are higher in both residual strain and average crack width due to the four-point bending test setup. The results obtained indicate that the beams damaged in the low strain level have a total crack width of size between 6 and 47 μm in the bottom line (5–37 μm in the middle line) and between 150 and 500 μm in the high strain level in the bottom line (60–300 μm in the middle line). These results show that the pre-cracking methodology proposed allows obtaining two different strain level groups, despite the difficulty of controlling an exact crack size.

Fig. 8 presents the relation between residual strain and the average crack width, both parameters measured at the bottom and middle DEMEC lines. The results are gathered in clear linear trends, which follow the equations shown in Fig. 9, with R2 values over 0.85. The trend obtained for C1 and C2 is different from the trend obtained for C3 and C4 concretes. Consequently, a strain level around 0.5‰ produces an average of around 10 μm for the UHPFRC samples and around 30 μm for the high-performance and conventional concrete samples. The presence of the crystalline admixture did not affect the trend in crack size vs strain noticeably.

3.3. Chlorides' penetration

All prisms were photographed after the cut to obtain the penetration profile of chlorides before and after healing. In most concrete groups, the samples gave lower penetration after healing than the samples before healing. Fig. 9 shows example pictures of C1, C2, C3, and C4 before and after healing.

Table 3 shows the values of the chlorides' penetration depth P_0, obtained per sample, which indicates the penetration of chlorides produced through the matrix. For the C1 samples, P_0 presents higher values than C2, C3, and C4 samples. C2 samples have only slightly higher P_0 than C3 and C4, due to the high quality of its matrix. In C3 and C4, the results show that before healing, only specimens damaged to the high strain level had consistently small matrix penetration of around 2–3 mm. The results also show that samples after healing had no penetration of chlorides, to the exception of one sample, that could have behaved as an outlier.

Table 4 shows the values of penetration of chlorides in the penetration branches detected in the profiles. The results show that C3-C4 samples damaged to the low strain level before healing have only 1 to 3 penetration branches, with a width between 1 and 6 mm, and after healing, no penetration branches were detected. Similarly, C3-C4 samples damaged to the low strain level have between 1 and 15 penetration branches, with an average width between 2 and 13 mm, while after healing, only 1–7 branches were detected, width a smaller width, between 1 and 6 mm. This result demonstrates the protection that autogenous healing of small cracks can produce against the penetration of chlorides. It needs to be mentioned that in one C1 sample the number of cracks made impossible to have an accurate measure of P_0.

In C1, penetration of the samples after healing (right column in Fig. 9. 10) is lower if compared with the penetration before healing (left column in Fig. 9. 10), and the penetration of chlorides along the sample width disappears. This result indicates that autogenous healing in conventional concretes such as C1 with small cracks is able to reduce the penetration of chlorides significantly after 1-month of healing in deionized water. There is still penetration in the uncracked areas, which presents a slight reduction if compared with the equivalent samples before healing, which indicates that the month inside water helped in the densification of the matrix and reduction of its permeability. For C2 samples, even for the large crack group, penetration through the matrix was not detected due to its denser matrix, and cracks were not detected through this method, which is thought to have been caused by

Table 2
Strain, average crack width, number of cracks, and total crack width per beam.

Strain level	Mix	Residual strain		Crack width Avg (std.dev)		Number of cracks		Total crack width	
		Bottom	Middle	Bottom	Middle	Bottom	Middle	Bottom	Middle
		(‰)	(‰)	(μm)	(μm)	–	–	(μm)	(μm)
Low strain	C1	0.48	0.22	29 (0)	28 (0)	1	1	29	28
		0.45	0.23	22 (0)	17 (0)	1	1	22	17
	C2	0.60	0.26	27 (0)	22 (0)	1	1	27	22
		0.42	0.20	24 (8.11)	19 (1.64)	2	2	47	37
	C3	0.71	0.33	11 (2.07)	9 (1.66)	3	3	32	26
		0.69	0.25	11 (0.38)	10(0)	3	1	32	10
	C31	0.5	0.24	9 (2.34)	5(0)	5	1	44	5
		0.41	0.22	8 (0.20)	9 (1.83)	2	2	16	18
	C4	0.44	0.18	6(0)	6 (0.7)	1	2	6	13
		0.5	0.27	10 (0.40)	8 (0)	2	2	19	17
	C41	0.62	0.23	8 (1.14)	10 (0)	2	1	17	10
		0.51	0.21	6 (0.90)	9 (1.70)	2	2	12	18
High strain	C1	3.70	1.66	200 (70.71)	100 (70.71)	2	2	400	200
		2.95	1.26	200 (35.36)	100 (35.36)	2	2	400	200
	C2	4.33	2.56	150 (57.74)	100 (57.74)	3	3	450	300
		4.33	2.78	250 (70.71)	150 (35.35	2	2	500	300
	C3	1.40	0.81	25 (7.07)	15 (7.07)	12	12	300	180
		1.55	0.90	25 (5.22)	15 (5.04)	11	11	275	165
	C31	1.71	0.84	25 (7.07)	15 (5.34)	12	7	300	105
		1.71	0.80	30 (5.35)	20 (5.47)	7	5	210	100
	C4	2.26	1.21	25 (7.07)	15 (5.22)	20	11	500	165
		2.19	1.56	36 (28.78)	27 (36.14)	14	10	500	270
	C41	2.05	1.15	29 (10.95)	15 (7.07)	6	5	175	75
		1.63	0.86	25 (7.07)	15 (5.47)	6	4	150	60

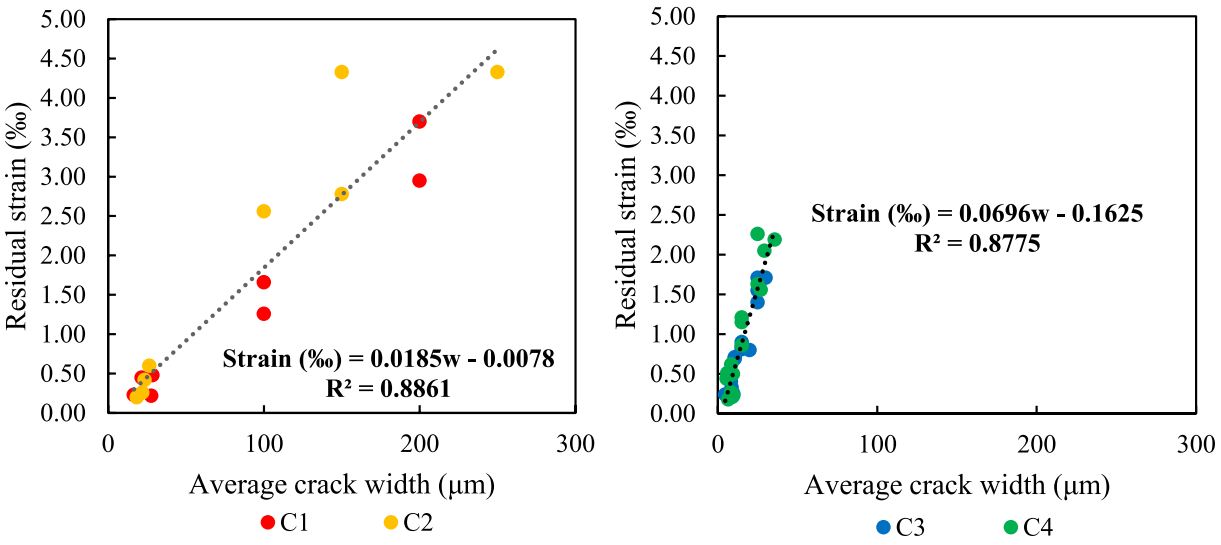

Fig. 8. Comparison of the residual strain and the average crack width obtained in all samples. Left graph for C1 and C2 beams and right graph for C3, C31, C4, and C41 beams.

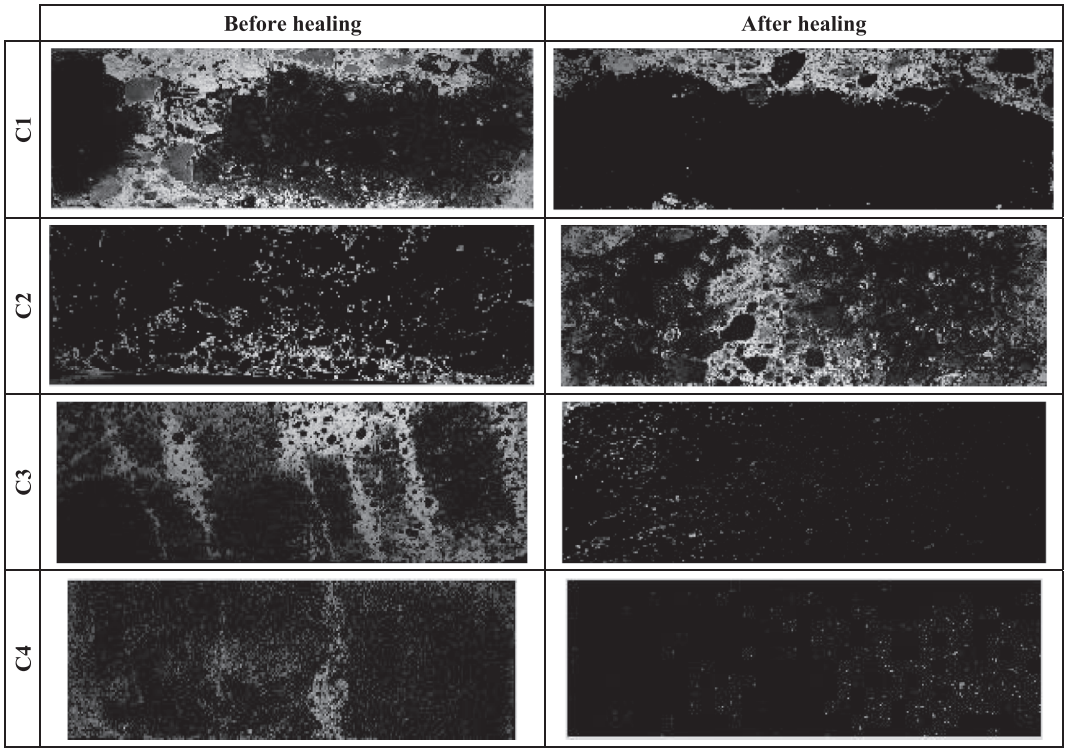

Fig. 9. Converted chloride penetration photos of C1, C2, C3, and C4 before and after healing.

uncontrolled cracking at the extreme parts of the beams.

C3 samples tested to the low strain suffered small cracks around 10 μm, and there were no macro cracks. The penetration through the matrix (P_0) is very small, undetectable for the low strain, and around 3 mm for the high strain levels before healing. After healing, this value is further improved, and no penetration through the matrix (P_0) could be detected. Similarly, there was no penetration in the samples of the C31 group loaded in the LS level, and the branches from the HS level disappeared after healing, indicating a complete self-healing, as happened in C3 samples.

In C4 samples, the penetration through the matrix (P_0) is very small and similar to C3 samples. However, the penetration branches obtained show different results. In the low strain levels, several branches of size around 5 mm were detected, in contrast to the lack of branches in C3. This penetration pattern disappeared after healing for the samples with the low strain level, but some branches remained for the high strain level after healing, as happened with C3 samples. For C41 samples, most of the penetration branches disappeared after healing. It should be mentioned that the penetration branches detected in C41 samples loaded to the high strain level were around two times wider than in C4, and the number of branches was 0.5 times smaller, suggesting a concentration of cracks in each branch.

Table 3
Chlorides' penetration depth P0, penetration through the matrix.

Mix	P_0 (mm)			
	Before Healing		After Healing	
	Low Strain	High Strain	Low Strain	High Strain
C1	7.58	–	10.27	–
C1	–	–	–	–
C2	4.94	–	0.0	–
C2	2.48	–	0.0	–
C3	0.0	2.5	0.0	0.0
C3	0.0	2.3	0.0	0.0
C31	3.3	2.5	0.0	0.0
C31	0.0	1.8	0.0	0.0
C4	2.7	2.5	0.0	0.0
C4	0.0	0.0	0.0	0.0
C41	0.0	2.6	0.0	7.0
C41	2.6	2.2	0.0	0.0

3.4. Quantification of self-healing

In order to evaluation of the self-healing capability of Eq. (1) was used with two parameters, the percentage of the area of penetration of chloride with respect to the whole area and the width of the penetration branches.

The healing ratio calculated using the percentage of area penetrated by chloride versus their residual strain is presented in Fig. 10 left. The residual strain values in the figure are the residual strain of the bottom line, which are more representative of residual strain in this work. The reason is, the creation of the crack starts from the bottom part, then maybe some cracks do not continue until the upper line. Fig. 10 depicts the decrement obtained in the healing ratio as residual strain increases. C1 and C2 samples damaged to the small strain level obtained healing ratios between 30 and 60%, while C3 and C4 mixes with comparable strain levels received almost 100% of healing. This improvement shows the benefit of multi-cracking in healing if compared with samples with similar total crack levels but concentrated in single cracks. In UHPFRC samples with residual strain values lower than 1‰, the healing efficiency is almost 100% in all samples.

In UHPFRCs, self-healing was also evaluated using the width of the penetration branches. Each sample's average penetration width was compared with its couple after healing according to their residual strain. Fig. 10 displays a descending healing ratio when increasing the residual strain in average penetration. Again, for residual strain lower than 1‰, the healing percentages were almost 100% in all cases. The healing ratios obtained for samples incorporating CA are slightly better than their reference, which indicates a potential enhancement of self-healing by this admixture.

Each penetration width was represented against their residual strain (Fig. 11) in order to compare the evolution of each penetration branch width, before and after healing. This representation was performed for

Table 4
Penetration values were obtained in the crack branches, including the number of branches (no.), the width of the branches (average and standard deviation).

Mix	Before healing						After healing					
	Low Strain			High Strain			Low Strain			High Strain		
	no.	Branch Width		no.	Branch Width		no.	Branch Width		no.	Branch Width	
		avg.*(mm)*	std.dev.*(mm)*		avg.*(mm)*	std.dev.*(mm)*		avg.*(mm)*	std.dev.*(mm)*		avg.*(mm)*	std.dev.*(mm)*
C3	0	–	–	5	4.5	3.9	0	–	–	5	6.2	0.6
C3	0	–	–	15	3.2	1.8	0	–	–	3	2.5	1.2
C31	0	–	–	1	2.4		0	–	–	1	1.1	–
C31	0	–	–	4	3.1	1.1	0	–	–	0	–	–
C4	2	3.6	3.4	8	3.1	1.3	0	–	–	5	5.5	3.9
C4	3	6.1	6.6	8	7.8	3.7	0	–	–	0	–	–
C41	0	–	–	5	12.4	6.4	0	–	–	7	5.9	3.7
C41	1	0.7	1.0	2	13.4	1.6	0	–	–	0	–	–

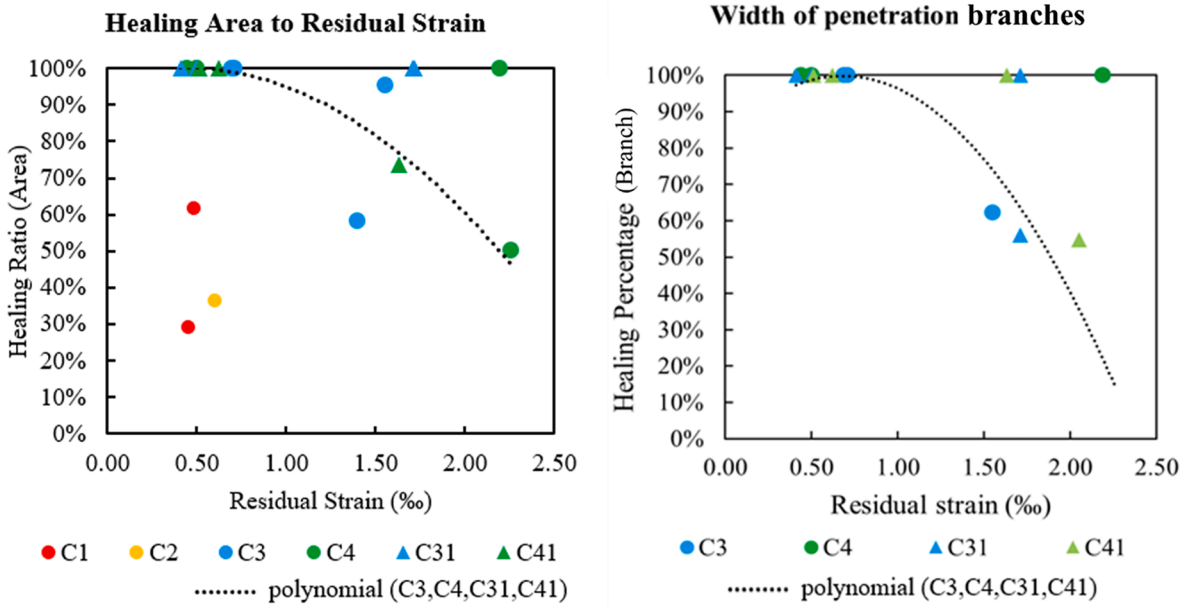

Fig. 10. Healing Ratio of area penetration (left) and width of penetration branch (right) vs. their residual strain in UHPFRC samples.

all the individual branches, depending on their residual strain. Fig. 11 left shows the values before healing, and Fig. 11 right after healing. The results show that increasing the strain increases the penetration width before and after healing. After healing, the penetration is noticeably reduced if compared with the samples before healing, especially for residual strains lower 1–1.4 ‰, which suggests a healing threshold for the conditions of this study.

3.5. Discussion

For conventional concrete samples (C1) and high-performance concrete samples (C2), because of their crack pattern of single wider cracks, the traditional water penetration test used in other studies [12,13,22] is applicable to analyze the permeability. The method proposed in this work has inherent difficulties for these concrete types due to the higher porosity of the matrix (P_0) and the crack localization, which is more randomized and difficult to predict than in UHPFRC samples (C3 and C4). Furthermore, the effect of CA on longer-term still needs to be studied as the crystallization process can be produced with better efficiencies at other ages. Additionally, the penetration produced through the matrix is similar to the penetration from the branch, and when this penetration is high (C1), the two processes may be mixed and hindered. Thus, the method presented is not the most appropriate for conventional and high-performance concrete samples. However, it allowed a general comparison width of UHPFRC samples with a similar residual strain level. Conversely, in UHPFRC samples, the penetration areas and pattern obtained were clear enough to detect the effects of self-healing significantly in samples with the high strain level. For samples with low strain levels, the precision of the method should be improved to distinguish better the phenomenon taking place. In fact, when the penetration through the matrix and the branches is very small, slight contamination with chlorides that may have been produced during the cutting process can play a role and hinder obtaining exact measurements on penetration. Moreover, to improve further the accuracy of the results, a dry cut process is recommended for subsequent studies.

Comparing with the results already published in the literature, crack widths of 10 μm are considered as a critical width to avoid chlorides' penetration in a structure [2]. However, in this study, UHPFRC samples with cracks around 10 μm (even smaller) experienced some chlorides penetration after being exposed for 3 days to a 50-cm water column containing sodium chloride. This result indicates that the penetration of chlorides happens even in very tight cracks produced in the multi-cracking pattern of UHPFRC. The study of the concentration of chlorides that penetrated through these tight cracks will be of interest to discern if that penetration detected is threatening or has no significant effect on UHPFRCs durability in the long term. However, in the conditions of this study, autogenous healing produced in water immersion promoted the protection of UHPFRCs healed samples from chlorides' penetration.

4. Conclusions

This study verified the alternative use of the measure of the penetration of chlorides for the evaluation of self-healing in elements with very low water permeability instead of previously used water permeability tests based on measuring a water flow. Specifically, this work studied autogenous healing in reinforced beams of conventional concrete, a high-performance concrete, and two types of UHPFRCs, and the enhanced autogenous healing of the two types of UHPFRCs with 0.8% of CA by the binder weight. The beams were pre-cracked until two predefined residual strain levels, and samples extracted from the center of the beams were used to evaluate self-healing using chlorides' penetration test as an indicator of water penetration. The conclusions that can be drawn are:

- The pre-cracking method allowed to obtain beams with comparable strain levels (total crack width) but with various average crack widths depending on their mix. For instance, in UHPFRC samples, the average crack widths obtained were around 10 μm for the low strain level and 25–50 μm for the high strain level. On the contrary, these values were 20–30 μm and 150–250 μm for high-performance and conventional concrete. In UHPFRC samples, the crack size dispersion is significantly lower than those for the other two mixes.
- In all the mixes, self-healing was evaluated by the percentage of area penetrated by chlorides. Conventional Concrete and High Performance Concrete samples with the small strain level obtained healing ratios between 30 and 60%, while UHPFRC mixes with comparable strain level, obtained almost 100% of healing. This improvement shows the benefit of multi-cracking in healing if compared with samples with similar total crack levels but concentrated in single cracks.
- In UHPFRC, self-healing was also evaluated by the width of the penetration branches along with the depth of the samples. UHPFRC mixes show excellent self-healing efficiency (with and without CA) until strains around 1‰. This means that samples damaged width smaller strain levels are able to heal in 28 days underwater immersion and obtain almost complete protection against penetration, with the parameters of this study. UHPFRC samples with higher strain levels had a decreasing healing performance with increasing residual strain values, and thus, the protection from chlorides' penetration is

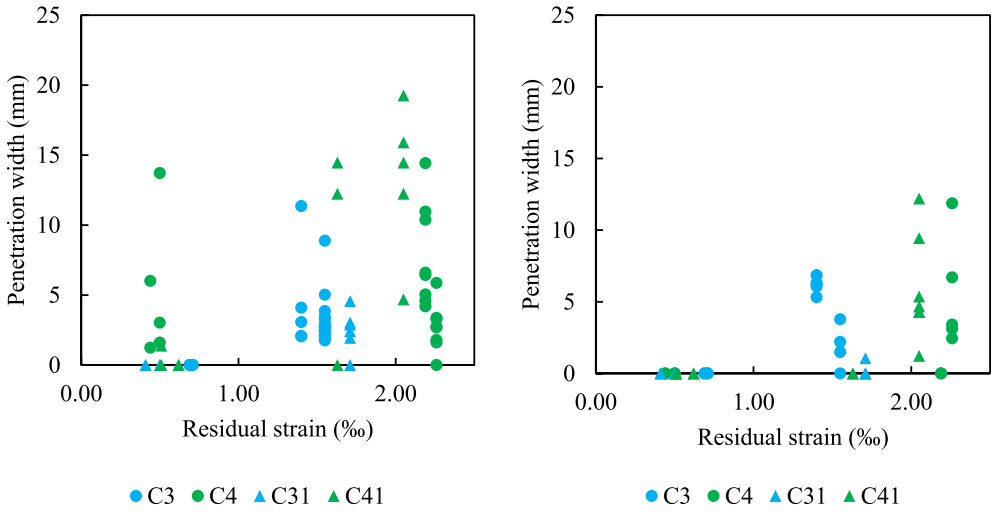

Fig. 11. Penetration width of all UHPFRC samples by their residual strain before (left) and after (right) self-healing.

reduced accordingly. No differences were detected from using CA by this method and conditions of the study; however, other conditions such as longer healing time can potentially produce better healing. The UHPFRC type with higher fiber content, demonstrated superior healing capability due to their better redistribution of stresses promoting multi-cracking.

CRediT authorship contribution statement

Hesam Doostkami: Conceptualization, Investigation, Writing – original draft, Writing – review & editing. **Marta Roig-Flores:** Methodology, Validation, Writing – review & editing. **Pedro Serna:** Supervision, Writing – review & editing, Conceptualization, Validation, Methodology, Resources, Funding acquisition.

Declaration of Competing Interest

The authors declare that they have no known competing financial interests or personal relationships that could have appeared to influence the work reported in this paper.

Acknowledgments

The activity described in this paper has been performed in the framework of the project "Rethinking coastal defence and Green-energy Service infrastructures through enHancEd-durAbiLity high-performance cement-based materials-ReSHEALience", funded by the European Union Horizon 2020 research and innovation programme under GA No 760824. The authors would also like to thank Sika and Penetron for providing materials for the tests and E.J. Mezquida-Alcaraz for the characterization of UHPFRC mixes with Inverse Analysis.

References

[1] N. De Belie, E. Gruyaert, A. Al-Tabbaa, P. Antonaci, C. Baera, D. Bajare, A. Darquennes, R. Davies, L. Ferrara, T. Jefferson, C. Litina, B. Miljevic, A. Otlewska, J. Ranogajec, M. Roig-Flores, K. Paine, P. Lukowski, P. Serna, J. M. Tulliani, S. Vucetic, J. Wang, H.M. Jonkers, A Review of Self-Healing Concrete for Damage Management of Structures, Adv. Mater. Interfaces. 5 (2018), https://doi.org/10.1002/admi.201800074.

[2] M. Maes, D. Snoeck, N. De Belie, Chloride penetration in cracked mortar and the influence of autogenous crack healing, Constr. Build. Mater. 115 (2016) 114–124, https://doi.org/10.1016/j.conbuildmat.2016.03.180.

[3] H.L. Wang, J.G. Dai, X.Y. Sun, X.L. Zhang, Characteristics of concrete cracks and their influence on chloride penetration, Constr. Build. Mater. 107 (2016) 216–225, https://doi.org/10.1016/j.conbuildmat.2016.01.002.

[4] J. Jiang, X. Zheng, S. Wu, Z. Liu, Q. Zheng, Nondestructive experimental characterization and numerical simulation on self-healing and chloride ion transport in cracked ultra-high performance concrete, Constr. Build. Mater. 198 (2019) 696–709, https://doi.org/10.1016/j.conbuildmat.2018.11.054.

[5] C. Edvardsen, Water permeability and autogenous healing of cracks in concrete, 1999.

[6] L. Ferrara, T. Van Mullem, M.C. Alonso, P. Antonaci, R.P. Borg, E. Cuenca, A. Jefferson, P.L. Ng, A. Peled, M. Roig-Flores, M. Sanchez, C. Schroefl, P. Serna, D. Snoeck, J.M. Tulliani, N. De Belie, Experimental characterization of the self-healing capacity of cement based materials and its effects on the material performance: A state of the art report by COST Action SARCOS WG2, Constr. Build. Mater. 167 (2018) 115–142, https://doi.org/10.1016/j.conbuildmat.2018.01.143.

[7] H.-W. Reinhardt, M. Jooss, Permeability and self-healing of cracked concrete as a function of temperature and crack width, Cem. Concr. Res. 33 (7) (2003) 981–985, https://doi.org/10.1016/S0008-8846(02)01099-2.

[8] American Concrete Institute Committee 212, Report on Chemical Admixtures for concrte, 2010.

[9] L. Ferrara, V. Krelani, F. Moretti, On the use of crystalline admixtures in cement based construction materials: From porosity reducers to promoters of self healing, Smart Mater. Struct. 25 (8) (2016) 084002, https://doi.org/10.1088/0964-1726/25/8/084002.

[10] K. Sisomphon, O. Copuroglu, E.A.B. Koenders, Self-healing of surface cracks in mortars with expansive additive and crystalline additive, Cem. Concr. Compos. 34 (4) (2012) 566–574, https://doi.org/10.1016/j.cemconcomp.2012.01.005.

[11] K. Sisomphon, O. Copuroglu, E.A.B. Koenders, Effect of exposure conditions on self healing behavior of strain hardening cementitious composites incorporating various cementitious materials, Constr. Build. Mater. 42 (2013) 217–224, https://doi.org/10.1016/j.conbuildmat.2013.01.012.

[12] M. Roig-Flores, F. Pirritano, P. Serna, L. Ferrara, Effect of crystalline admixtures on the self-healing capability of early-age concrete studied by means of permeability and crack closing tests, Constr. Build. Mater. 114 (2016) 447–457, https://doi.org/10.1016/j.conbuildmat.2016.03.196.

[13] M. Roig-Flores, S. Moscato, P. Serna, L. Ferrara, Self-healing capability of concrete with crystalline admixtures in different environments, Constr. Build. Mater. 86 (2015) 1–11, https://doi.org/10.1016/j.conbuildmat.2015.03.091.

[14] E. Cuenca, A. Tejedor, L. Ferrara, A methodology to assess crack-sealing effectiveness of crystalline admixtures under repeated cracking-healing cycles, Constr. Build. Mater. 179 (2018) 619–632, https://doi.org/10.1016/j.conbuildmat.2018.05.261.

[15] R.P. Borg, E. Cuenca, E.M. Gastaldo Brac, L. Ferrara, Crack sealing capacity in chloride-rich environments of mortars containing different cement substitutes and crystalline admixtures, J. Sustain. Cem. Mater. 7 (3) (2018) 141–159, https://doi.org/10.1080/21650373.2017.1411297.

[16] K. Habel, P. Gauvreau, Response of ultra-high performance fiber reinforced concrete (UHPFRC) to impact and static loading, Cem. Concr. Compos. 30 (10) (2008) 938–946, https://doi.org/10.1016/j.cemconcomp.2008.09.001.

[17] J.-P. Charron, E. Denarié, E. Brühwiler, Permeability of ultra high performance fiber reinforced concretes (UHPFRC) under high stresses, Mater. Struct. Constr. 40 (3) (2007) 269–277, https://doi.org/10.1617/s11527-006-9105-0.

[18] K. Habel, J.-P. Charron, E. Denarié, E. Brühwiler, Autogenous deformations and viscoelasticity of UHPFRC in structures. Part I: Experimental results, Mag. Concr. Res. 58 (3) (2006) 135–145, https://doi.org/10.1680/macr.2006.58.3.135.

[19] K. Habel, Structural Behaviour of Elements Combining Ultra-High Performance Fibre Reinforced Concretes (Uhpfrc) and Reinforced Concrete, Fifth RILEM Symp, Fibre-Reinforced Concr. - BEFIB' 2000 (2004), https://doi.org/10.5075/epfl-thesis-3036.

[20] M. Valcuende, J.R. Lliso-Ferrando, M. Roig-Flores, J.M. Gandía-Romero, Porous Structure of ultra-high-performance fibre-reinforced concretes, Materials (Basel). 14 (7) (2021) 1637, https://doi.org/10.3390/ma14071637.

[21] M.G. Sohail, R. Kahraman, N. Al Nuaimi, B. Gencturk, W. Alnahhal, Durability characteristics of high and ultra-high performance concretes, J. Build. Eng. 33 (2021) 101669, https://doi.org/10.1016/j.jobe.2020.101669.

[22] A. Negrini, M. Roig-Flores, E.J. Mezquida-Alcaraz, L. Ferrara, P. Serna, M. G. Grantham, C. Mircea, Effect of crack pattern on the self-healing capability in traditional, HPC and UHPFRC concretes measured by water and chloride permeability, MATEC Web Conf. 289 (2019) 01006, https://doi.org/10.1051/matecconf/201928901006.

[23] K. Wang, D.C. Jansen, S.P. Shah, A.F. Karr, Permeability study of cracked concrete, Cem. Concr. Res. 27 (3) (1997) 381–393, https://doi.org/10.1016/S0008-8846(97)00031-8.

[24] S. Granger, G. Pijaudier-Cabot, A. Loukili, Mechanical behavior of self-healed Ultra High Performance Concrete: From experimental evidence to modeling, Proc. 6th Int, Conf. Fract. Mech. Concr. Concr. Struct. 3 (2007) 1827–1834.

[25] C. Desmettre, J.-P. Charron, Water permeability of reinforced concrete with and without fiber subjected to static and constant tensile loading, Cem. Concr. Res. 42 (7) (2012) 945–952, https://doi.org/10.1016/j.cemconres.2012.03.014.

[26] P. Escoffres, C. Desmettre, J.P. Charron, Effect of a crystalline admixture on the self-healing capability of high-performance fiber reinforced concretes in service conditions, Constr. Build. Mater. 173 (2018) 763–774, https://doi.org/10.1016/j.conbuildmat.2018.04.003.

[27] B. Šavija, E. Schlangen, Autogeneous healing and chloride ingress in cracked concrete, Heron. 61 (2016) 15–32.

[28] M. Ismail, A. Toumi, R. François, R. Gagné, Effect of crack opening on the local diffusion of chloride in cracked mortar samples, Cem. Concr. Res. 38 (8-9) (2008) 1106–1111, https://doi.org/10.1016/j.cemconres.2008.03.009.

[29] N. Otsuki, S. Nagataki, K. Nakashita, Evaluation of the AgNO3 solution spray method for measurement of chloride penetration into hardened cementitious matrix materials, Constr. Build. Mater. 7 (4) (1993) 195–201, https://doi.org/10.1016/0950-0618(93)90002-T.

[30] V. Baroghel-Bouny, P. Belin, M. Maultzsch, D. Henry, AgNO3 spray tests: Advantages, weaknesses, and various applications to quantify chloride ingress into concrete. Part 2: Non-steady-state migration tests and chloride diffusion coefficients, Mater. Struct. Constr. 40 (8) (2007) 783–799, https://doi.org/10.1617/s11527-007-9236-y.

[31] L.V. Real, D.R.B. Oliveira, T. Soares, M.H.F. Medeiros, Método colorimétrico por aspersión de nitrato de plata para la evaluación de la penetración de cloruros en concreto: estado del arte, Rev. ALCONPAT. 5 (2015) 149–159, https://doi.org/10.21041/ra.v5i2.84.

[32] I.-S. Yoon, E. Schlangen, Experimental examination on chloride penetration through micro-crack in concrete, KSCE J. Civ. Eng. 18 (1) (2014) 188–198, https://doi.org/10.1007/s12205-014-0196-9.

[33] J.Ángel. López, P. Serna, J. Navarro-Gregori, E. Camacho, An inverse analysis method based on deflection to curvature transformation to determine the tensile properties of UHPFRC, Mater. Struct. Constr. 48 (11) (2015) 3703–3718, https://doi.org/10.1617/s11527-014-0434-0.

[34] J.Á. López, Characterisation of the Tensile Behaviour of Uhpfrc By Means of Four-Point Bending Tests, (2017). https://doi.org/10.4995/Thesis/10251/79740.

[35] E.J. Mezquida-Alcaraz, J. Navarro-Gregori, P. Serna-Ros, Direct procedure to characterize the tensile constitutive behavior of strain-softening and strain-hardening UHPFRC, Cem. Concr. Compos. 115 (2021) 103854, https://doi.org/10.1016/j.cemconcomp.2020.103854.

[36] M.A.R. Collepardi, 2 Quick Method To Determine Free and, 10 (1995) 10–16.
[37] E. Meck, V. Sirivivatnanon, Field indicator of chloride penetration depth, Cem. Concr. Res. 33 (8) (2003) 1113–1117, https://doi.org/10.1016/S0008-8846(03)00012-7.
[38] F. He, C. Shi, Q. Yuan, C. Chen, K. Zheng, AgNO3-based colorimetric methods for measurement of chloride penetration in concrete, Constr. Build. Mater. 26 (1) (2012) 1–8, https://doi.org/10.1016/j.conbuildmat.2011.06.003.